Journal of Applied Fluid Mechanics, Vol. 17, No. 4, pp. 799-815, 2024.
Available online at www.jafmonline.net, ISSN 1735-3572, EISSN 1735-3645.
https://doi.org/10.47176/jafm.17.4.2256

Investigating the Impact of Back Cavity Filling and Axial Clearance on the Flow Physics and Performance of a Pump as Turbine

R. Gaji[1], A. Doshi[2] and M. Bade[2†]

[1] *Sardar Vallabhbhai National Institute of Technology, Surat 395007, India /Annasaheb Dange College of Engineering and Technology, Ashta 416301, India*
[2] *Sardar Vallabhbhai National Institute of Technology, Surat 395007, India*

†Corresponding Author Email: bmh@med.svnit.ac.in

ABSTRACT

The Pumps as Turbines (PAT) is a well-established technology suitable for standalone micro-hydropower plants and energy recovery systems. But being lower performance than the dedicated turbines, there are continuous efforts to improve it keeping cost benefits intact. One of the recent modifications of the back cavity filling plays a crucial role in the performance of PAT which is not investigated in detail. In the present paper, the PAT back cavity is filled with a solid ring of various sizes and shapes (back cavity filling) to explore its impact. The developed test facility is used to validate the experimental results with the numerical results for the base case. A numerical model after validation has been employed to investigate the impact of back cavity filling on the internal flow dynamics and the PAT performance. Additionally, the study explored the influence of axial clearance on flow physics, associated losses, and the PAT performance, an aspect rarely discussed by researchers in the PAT mode. After back cavity filling, secondary flow-based disk friction losses were reduced, leading to a 3.5 % increase in PAT efficiency. An analysis of the axial clearance showed that increasing it from 0.015 to 0.076 (mean axial gap/impeller radius) led to a 2.6 % reduction in PAT efficiency. This decline can be primarily attributed to elevated losses associated with disk friction, increased volumetric losses, and the formation of a mixing zone at the impeller inlet, which impeded the flow into the impeller's flow zone.

Article History

Received August 21, 2023
Revised November 1, 2023
Accepted November 17, 2023
Available online January 30, 2024

Keywords:

Back cavity filling
Internal Hydraulics
Performance
Wake
Disk friction losses
Mixing zone

1. INTRODUCTION

Micro hydropower systems in the range of 5 to 100 kW provide a reliable and renewable energy solution for small-scale applications with ecological balance. For this application, pumps operated in reverse mode i.e. pump as turbine (PAT) is a practical and cost-effective proven solution compared to the dedicated turbine design and manufacturing due to its high cost (Binama et al., 2017). PAT utilizing pumps readily available in various specifications (head and discharges) are widely used for pressure reduction and energy recovery in various applications such as water distribution, sewage systems, reverse osmosis, etc.

One of the critical issues with PATs is they have a lower efficiency compared to conventional turbines due to various reasons such as it is not dedicatedly designed as turbine, the lack of a flow-controlling mechanism (Singh, 2005), etc. To compensate for the lower efficiency of PATs, researchers have focused on enhancing PAT performance through cost-effective geometric modifications. These include rounding the impeller blade tip and shroud edges to improve internal hydraulics, resulting in a collective increase in PAT efficiency by 1-2.5 % (Suarda et al., 2006; Singh & Nestmann, 2011; Doshi et al., 2017; Yang et al., 2021; Gaji et al., 2023). Adjustments to the impeller inlet diameter have been explored for different operating conditions, although a decrease in impeller diameter reduces PAT efficiency (Yang et al., 2012a). Singh (2005) proposed a systematic approach for performance enhancement and reported a series of simple modifications such as the introduction of an external stationary ring, suction eye enlargement, and removal of the eye rib from the volute to decrease swirl loss, leading to a 1.5 % increase in PAT efficiency in some cases or few PATs without much reliability, which are mainly covering main flow-zone (refer Fig. 1).

Nomenclature

C	absolute velocity
E	Euler
g	gravitational acceleration
H	net head
h	head
Q	discharge
T	torque
u	tangential blade velocity
GREEK SYMBOL	
Δ	difference
η	efficiency
ρ	mass density
ω	angular velocity

ABBREVIATIONS	
BEP	Best Efficiency Point
CFD	Computational Fluid Dynamics
PAT	Pump as Turbine
rpm	revolution per Minute
SUBSCRIPTS	
1	impeller inlet (Turbine mode)
2	impeller outlet (Turbine mode)
L	losses
u	tangential component
fz	flow zone
nfz	non-flow zone

Few years back, Doshi et al. (2018) introduced a novel modification called back cavity filling (BCF) for improving PAT efficiency, principally in non-flow zone region. BCF involves inserting a solid component into the back cavity as shown in Fig.1, which reduces disk friction losses. This modification resulted in a PAT efficiency improvement of 1.3 % (medium specific speed PATs) to 3.6 % (low specific speed PATs). The authors recommended need for further investigation using numerical tools to understand the changes in internal hydraulics and visualize the flow physics. Such insights in these phenomena will be helpful to evaluate the change in the performance and optimal operating parameters appropriately.

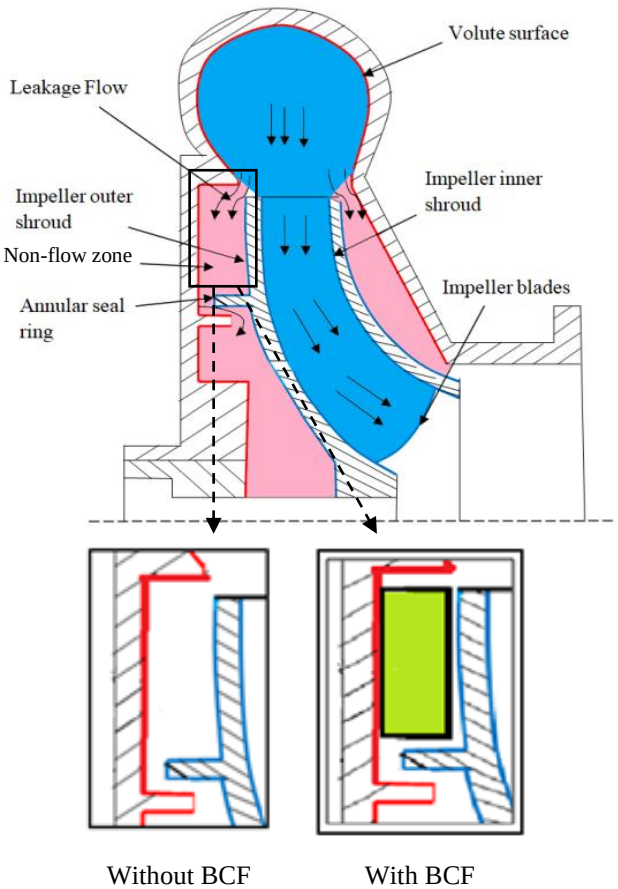

Fig. 1 PAT flow control volume without BCF and with BCF (Doshi, 2018)

Details of back cavity and related literature:

Generally, the pump manufacturers adopt various designs for the back cavity based on mechanical requirements, component standardization, manufacturing considerations, and cost factors (Zemanová & Rudolf, 2020). Similar to pump mode, in turbine mode also, the axial clearance is an important geometric parameter that impacts PAT performance (Zemanová & Rudolf, 2020). Consequently, optimizing the size and shape of the back cavity is crucial for achieving optimal PAT performance (Doshi, 2018). Although the detailed study of the influence of axial clearance on PAT performance and flow physics is limited, studies investigating the influence of axial clearance on pump and turbine performance are available in open literature. These studies are reviewed to get valuable insights into understanding the impact of axial clearance on internal hydraulics and performance for further evaluations.

The ratio of mean axial clearance to impeller radius in a pump is typically maintained between 0.03-0.08 to accommodate different impeller sizes within the volute (Gülich, 2013). It is important to note that the clearance passage is typically kept between 1-2 mm to minimize disk friction and volumetric losses for water turbines (Gülich, 2013). Yan et al. (2019) numerically evaluated the pump performance in both pump and reverse modes (specific speed 39.8 rpm) considering different clearance gaps of the labyrinth seal at the front cavity for pumped storage power plant applications. It is concluded that the turbine mode performance of a pump is more adversely affected by leakage losses compared to pump mode with the same clearance passage. The shape and axial clearance of a back cavity in a centrifugal pump not only affect the flow at non-flow zones but may disturb the impeller main flow zone (Doshi, 2018). Ayad et al. (2015) reported that an increase in the axial clearance of the back cavity resulted in a reduction in both the head and efficiency of a centrifugal pump.

In recent years, Computational Fluid Dynamics (CFD) software has gained extensive popularity for visualizing and comprehending the performance and flow characteristics of pumps, as a cost-effective alternative to relying on expensive experimental facilities (Li et al. 2023b). Numerical simulations, such as those by Yang et al. (2012b) shown that incorporating splitter blades increases efficiency by 3.42 %. Yang et al. (2014)

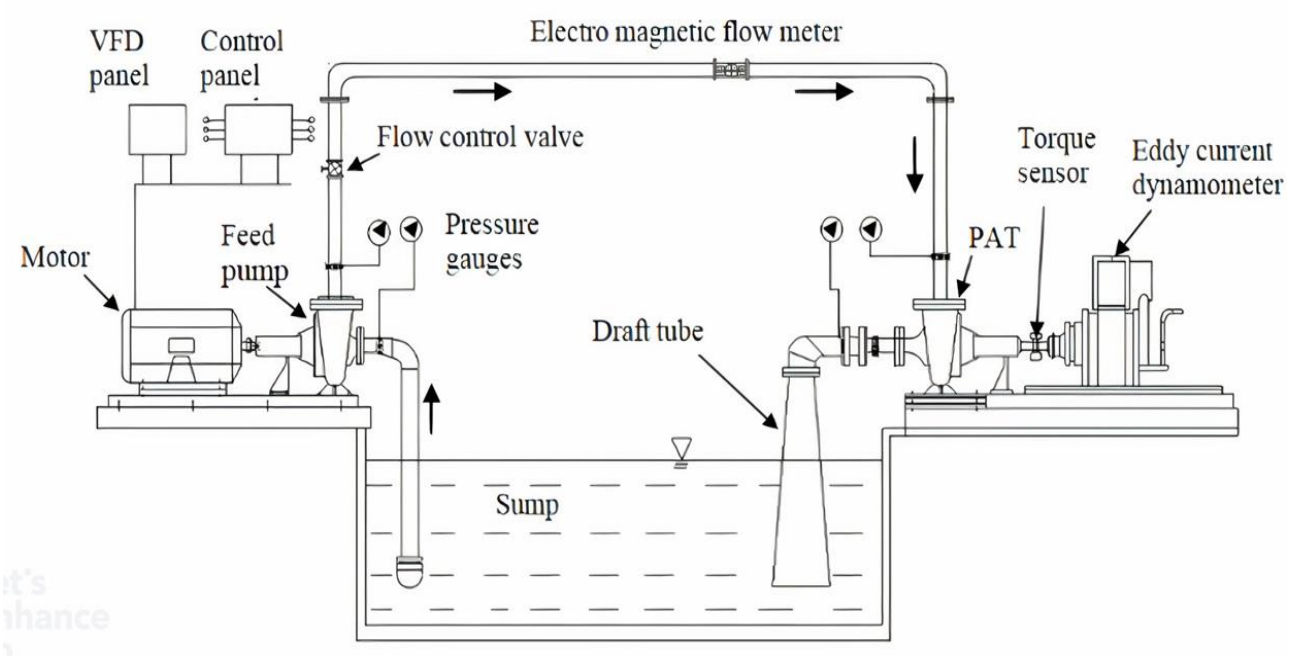

Fig. 2 Schematic of PAT test rig (Doshi et al. 2018)

Table 1 Main dimensions of impeller and volute

Parameters	Value	Parameters	Value
Inlet diameter of impeller (mm)	260	Shroud thickness (mm)	5
Outlet diameter of impeller (mm)	100	Blade angle at inlet (^{0})	21.7
Blade thickness (mm)	3.4	Number of blades	5
Impeller inlet width (mm)	15.5	Volute inlet dimeter (mm)	67

suggested that optimizing the radial gap between the impeller tip and the volute tongue can enhance PAT performance by up to 0.5 %. Researchers, including Miao et al. (2015) and Tian et al. (2019), have utilized CFD-based optimization techniques to determine optimal performance parameters. For example, Miao et al. (2015) achieved a 2.9 % efficiency improvement through blade profile optimization, while Tian et al. (2019) identified the optimal impeller configuration for maximum efficiency using CFD simulations and orthogonal test methods. These studies demonstrate that CFD tools are effective in analyzing qualitatively and quantitatively the influence of BCF, axial clearance, and other parameters on PAT performance.

This study addresses the need for detailed investigations of BCF in PAT systems through both experimental and computational approaches. A custom test rig is utilized to compare the performance of PAT with and without BCF. Experimental data is then used to validate a numerical model, ensuring its accuracy. With the validated numerical model, the study of the impact of BCF on the internal hydraulics of the PAT system is explored in detail. In this study, the influence of axial clearance in the back cavity on internal hydraulics and PAT performance is determined. The overall goal of the study is parametric analysis of the back cavity filling to find the optimal geometric configuration of filling material and to gain a comprehensive understanding of the internal hydraulics of it for enhancing PAT efficiency.

2. EXPERIMENTAL SETUP

To assess the impact of BCF, a state-of-the-art testing facility was established, as presented in Fig. 2 (Doshi et al., 2018). On this test facility, a low specific speed (19.9 rpm) [$N_{qp}=NQ^{1/2}/H^{3/4}$ (m, m^3/s)] end suction centrifugal pump was run in reverse mode, as it was already available in laboratory and had maximum improvement in efficiency. The parameters at experimentally determined best efficiency point (BEP) for this particular PAT operating in pump mode are a flow rate of 17.5 liters per second and a head of 20.4 meters, with a rotational speed of 1450 rpm. The important geometrical dimensions of the impeller and volute of PAT are presented in Table 1. The feed pump at various heads and flow rates supplied water to PAT, which is passed through the impeller to get mechanical energy and then discharged appropriately into tail race tank via draft tube. The loading on the PAT is performed through an eddy current dynamometer.

The test rig was equipped with sophisticated measuring instruments to capture external parameters, such as pressure transmitters, speed sensor, torque sensor, and a magnetic flow meter to measure pressure, speed, torque, and flow rate, respectively. The instrument specifications presented in Table A1 and Table A2 of Appendix indicate they are highly precise having very less value of uncertainty, which is important to justify the change in various performance parameters. The test

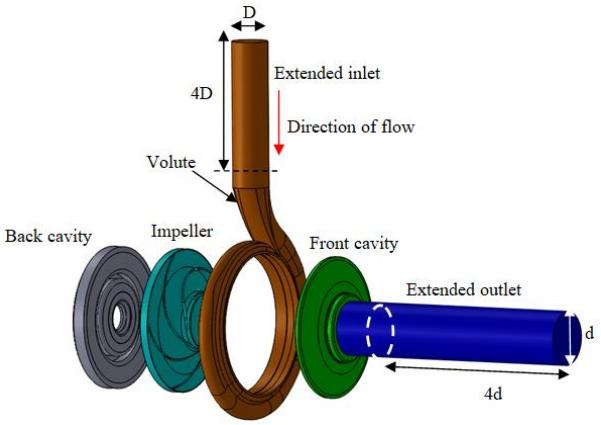

Fig. 3 Exploded view of PATcomputational model

facility shows excellent repeatability as indicated in Fig. A1 of Appendix. For automatic control and data acquisition, the experimental setup was supported by a Programmable Logic Controller (PLC) and SCADA software. The tests were conducted for both configurations, without BCF and with BCF stage. The obtained results are presented in the form of characteristic curves, showcasing the performance of the PAT.

3. NUMERICAL SIMULATION

3.1 Computational Model

The initial step in numerical simulation involves creating a computational model of the PAT, which encompasses the volute, front cavity, impeller, and back cavity, as depicted in Fig. 3. One of the critical components in the modelling is measurement and drafting of the actual size and shape of the front and back cavities so that it can be truly reflected in model depicting close to the reality to showcase actual flow physics, associated losses, and PAT performance.

Furthermore, volumetric losses and mechanical losses due to disk friction are considered in the simulation to accurately capture the behavior of the flow (Yang et al., 2012c). To ensure stable flow in the PAT, it is crucial to extend the length of both the inlet and outlet by a factor of four times their respective diameters. (see Fig. 3)(Cheng et al., 2023). For the configuration without BCF, the base model (model without BCF) is used, while, in the case of the model with BCF stage the back cavity is filled with a solid ring as shown in Fig. 4. The outer diameter of the solid ring is set to 260 mm, which is equal to the inlet diameter of the impeller. The computational model after incorporating the BCF modification is depicted in Fig. 5.

3.2 Generation of Mesh

The finite volume method is employed for discretization, utilizing tetrahedral mesh elements to represent the intricate flow domain. Mesh inflation is provided at the boundaries and impeller blades are refined to accurately capture the flow behaviour at the boundary wall. In order to determine the minimum number of mesh elements required, a mesh sensitivity test is conducted. The head

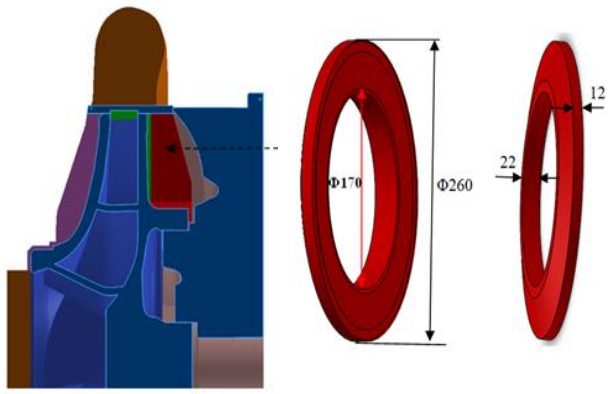

(a) (b)

Fig. 4 PAT with BCF specifications (a) position of BCF component (b) solid ring as a filling component

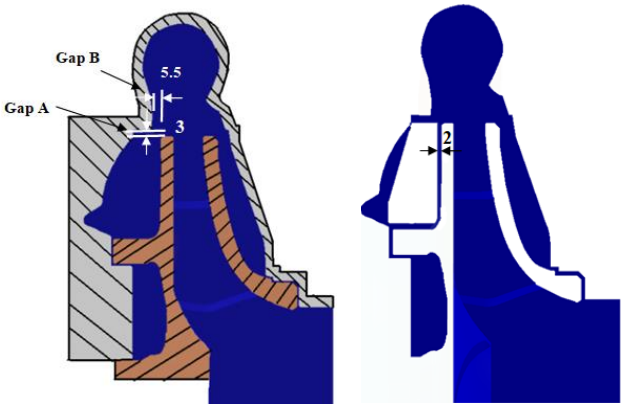

(a) (b)

Fig. 5 PAT model (a) geometric parameters (without BCF) and (b) computational model with BCF at meridional plane

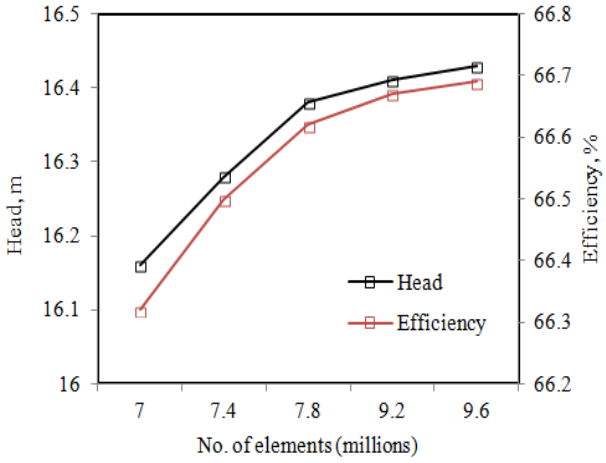

Fig. 6 Mesh sensitivity analysis

and efficiency are assessed by altering the number of elements at the designed flow rate (Q=16.9 lps) as presented in Fig. 6. Convergence is attained with 9,200,000 elements, resulting in minor deviations of 0.12 % in head and 0.02 % in efficiency. The total number of elements for the volute, impeller, and cavities are 4,140,000, 3,220,000, and 1,840,000 respectively. The meshing of different components of the PAT is depicted in Fig. 7.

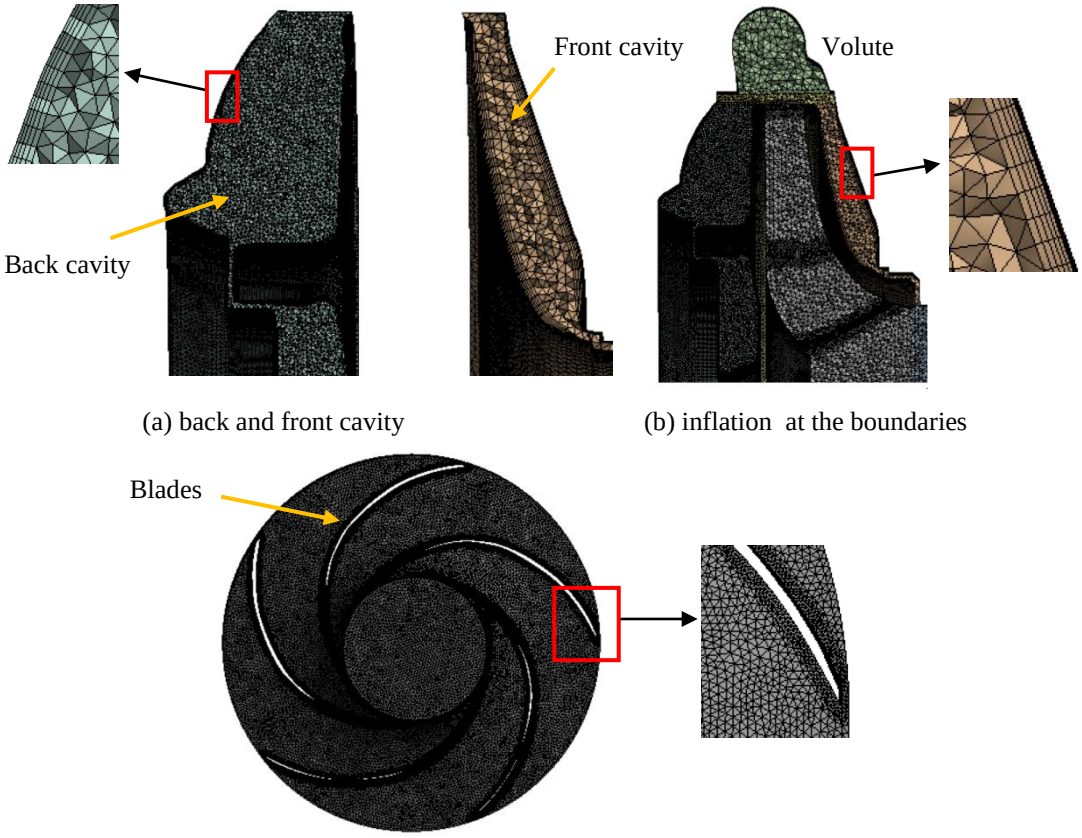

(a) back and front cavity

(b) inflation at the boundaries

(c) refinement at impeller blade

Fig. 7 Meshing of PAT components

To ensure proper resolution of the boundary layer by the mesh, the y+ value near the boundary wall is consistently kept at 2. This value is chosen to ensure simulation results near the wall are capturing actual flow physics.

3.3 Numerical Solution

To solve the Reynolds-averaged Navier-Stokes (RANS) equations, the CFD commercial software Ansys-Fluent (2022 R2) is utilized with working fluid for the simulation as water at normal temperature. The k-ω SST turbulence model is comparatively better in capturing flow recirculation, boundary layer effect in adverse pressure gradient for rotational flows than other conventional turbulence models (Javadi & Nilsson, 2017, Gaji et al., 2023; Li et al., 2023a, 2023c). In this simulation, the closure of the governing equations and boundary conditions involves utilizing pressure inlet and mass flow outlet conditions, which are set to match the experimental values across all flow rates, ranging from part load to overload regions.The surface roughness is another important parameter influencing PAT performance (Zariatin et al., 2019) but, generally, it was not accounted in the analysis by the researchers. In this study, the surface roughness measurements for the volute, internal and external surfaces of the impeller shroud, and impeller blades (as shown in Fig. 1) yielded values of 8.37 µm and 6.37 µm, respectively, using a surface roughness tester.

Given that the impeller's rotational speed is fixed at 1000 rpm, consistent with the experimental conditions, the outer surfaces of the shroud are prescribed a rotating wall boundary condition set at the same speed as the impeller.The volute, back cavity, and front cavity are set to a stationary frame, while the impeller is set to a rotating frame by frozen rotor approach (multiple reference frame model) at a speed of 1000 rpm. Total of 16 steady-state numerical simulations for different configurations without and with BCF are performed for each parameter of characteristics curves as head, torque, and efficiency by varying the discharge from part load to overload regions. First, the numerical model using Ansys-Fluent is validated with the experimental results previously obtained and then this validated model is used for simulation by varying the thickness of the filling material fixed on the volute in the back cavity to optimize its size as discussed in the following sections.

4. RESULTS AND DISCUSSION

In the section 4.1, the numerical results obtained for both the stages, without BCF and with BCF are validated by comparing them with experimental results. Further, in section 4.2, trend of the characteristics curve are explained in details. Section 4.3 utilizes the validated numerical model to investigate and present the flow physics at three different operating conditions: BEP, part load, and overload.This simulation study is extended in Section 4.4 presenting the influence of axial clearance on internal hydraulics and the performance of the PAT.

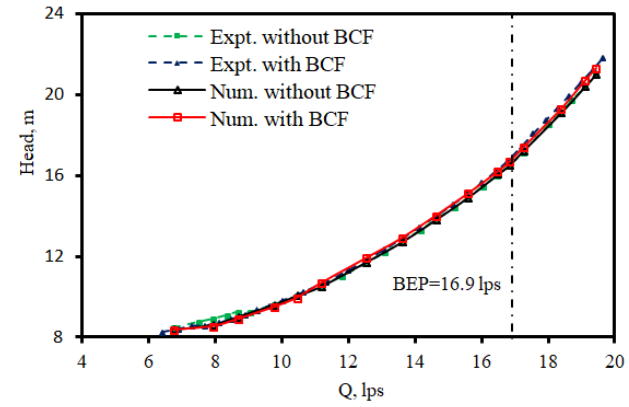

a) Head Vs Q

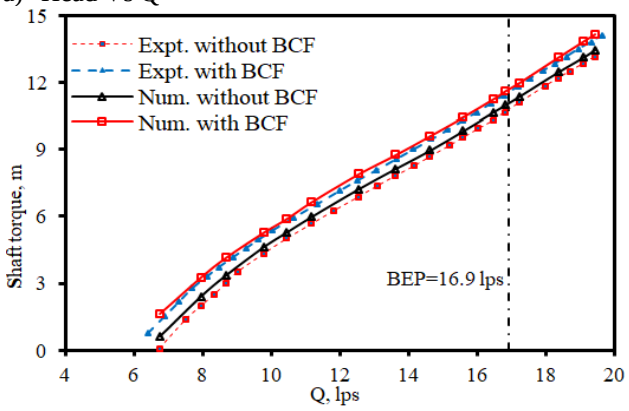

b) Shaft torque Vs Q

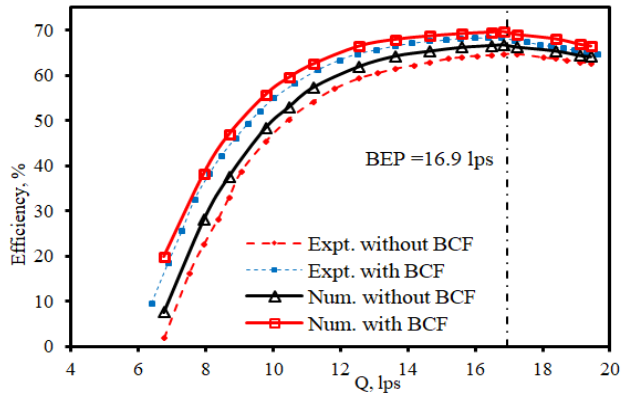

c) Efficiency Vs Q

Fig. 8 PAT characteristics with experimental and numerical approach

4.1 Validation of the Numerical Results

The numerical results for both, with and without BCF stages are compared with the experimental results, presented as a characteristic curves for 19.9 rpm PAT, as depicted in Fig. 8. Specifically, the numerical head curve closely overlaps with the experimental head curve. While, the numerical shaft torque and efficiency curves are consistently higher than their respective experimental curves, primarily because the mechanical losses at the bearing and shaft are challenging to account appropriately and hence not considered in the numerical simulation, (Yang et al., 2012c).

In this work, the maximum deviation noticed is 6.6 % with respect to experimental for the case of the shaft torque (refer Table 2), which is quite less than the permissible limit as per the literature (Gulich, 2013). The numerically deduced head seems to be lower than the respective experimental by a very small margin (1.1 %) in the part load region. At BEP and overload conditions, the maximum deviation is 3.3 % and 3 % with experimental efficiency and shaft torque, respectively. Overall, the proposed numerical model of the PAT at 19.9 rpm is validated by comparing characteristics curves from experimental and numerical investigations, with and without BCF (Fig. 8). The agreement between the curves confirms the model's accuracy in predicting the PAT's performance.

4.2 Discussion on Characteristic Curves Without and With BCF

All three characteristics curves, Head, shaft torque, and efficiency Vs. discharge (Q) show standard trend both for experimental and simulation results of 19.9 rpm PAT. Analyzing the Head Vs Q curve in Fig. 8 (a), it is observed that both curves, the experimental and numerical head for the without and with BCF stage are having very small margin throughout.

In the shaft torque vs. Q curve, both the numerical and experimental shaft torque curves for the with BCF stage are consistently above the respective curve of the without BCF stage throughout the operating range, with a positive margin. The efficiency vs. Q graph follows similar trend as that of shaft torque curve as summarized in Table 2. The margin of efficiency improvement at part load condition is greater than that at overload condition by visibal difference. The improvement in performance due to BCF by material of appropriate shape and size is justified by numerical simulation also by the approximately same margin as proposed by Doshi et al. (2018). Further, they have proposed the mixing theory at mixed zone (entry of the impeller near volute tounge in PAT mode) and supported by analytical model. It is interesting to varify it by numerical model understanding the flow physics of it, which is discussed in the following sections.

4.3 Internal Hydraulics of PAT Due to BCF

In this section, the numerical results are discussed with the help of change in the internal flow physics along with the theoretical model proposed in the literature (Doshi et al., 2018) and model equations (B1)-(B5) are reproduced as shown in Appendix for 19.9 rpm PAT without and with BCF modifications.

4.3.1 Flow Physics in the Back Cavity at BEP

The shape and size of the back cavity with radial and axial distances with volute tongue and impeller tips (Gap A and B presented in Fig. 5) are important parameters for internal flow hydraulics. For the selected PAT, the radial gap between volute tongue and impeller inlet (Gap A) is 3 mm, and the axial clearance between volute and impeller back shroud at the volute tongue (Gap B) is 5.5 mm [refer Fig. 5 (a)]. From this space, water from the back cavity is very well able to interact with the incoming fluid, which forms two interesting phenomena (Doshi et al. 2018) of flow physics as mentioned followings:

Table 2 PAT performance at without and with BCF stage at different operating condition

			Without BCF			With BCF		
	Flow rate (lps)	Results	Numerical	Expt.	Deviation (%)	Numerical	Expt.	Deviation (%)
Part load condition	8.7	Head (m)	9.1	9.2	-1.1	8.9	9	-1.1
		Shaft Torque (m)	3.2	3	+6.6	4.1	3.9	+5.1
		Efficiency (%)	35.1	33.1	+6	46.3	44.2	+5.1
BEP	16.9	Head (m)	16.4	16.72	-1.91	16.59	17.02	-2.52
		Shaft Torque (m)	11	10.79	+1.94	11.6	11.58	-0.17
		Efficiency (%)	66.7	64.55	+3.33	70.2	68.14	+3.02
Overload condition	19.1	Head (m)	20.5	20.4	+0.5	20.7	20.6	+0.4
		Shaft Torque (m)	13.1	12.84	+2	13.8	13.4	+3
		Efficiency (%)	64.4	63	+2.2	67	65.6	+2.1

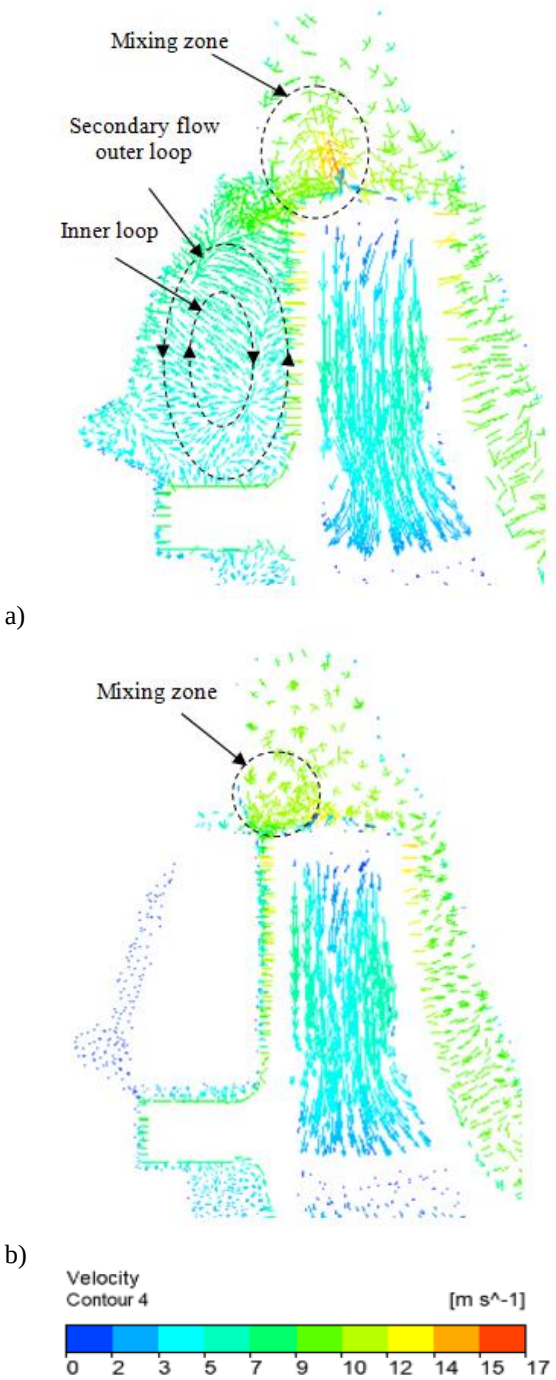

Fig. 9. Velocity vector plot at the PAT meridional plane at BEP (a) without BCF and (b) with BCF

1) Secondary flow and disk friction losses: Due to the no-slip condition, there is an interesting boundary layer formation, as one end of water is revolving at the impeller velocity and the other side (volute) is stationary having zero velocity. Due to this, the centrifugal force is imposed on the fluid in contact with the outer shroud of an impeller, forcing the fluid to move radially outward. On the other hand, the high pressure fluid supplied from volute moves in radially inwards, as per the continuity equation as shown in Fig. 9 (a), also trying to move in the back cavity present between the outer shroud and volute. This leads to the formation of large secondary flow-based disk friction losses. These losses contribute to energy dissipation as they decelerate the impeller reducing the torque generated due to water force and affect adversely on the overall performance of the PAT. Similar to above mentioned internal flow physics was explained by Gulich (2003) for both directions of velocity components as, radially outwards and tangential to a rotational plane, but for pump operation. In the case of the PAT, the flow physics is different from the pump in the mixing regions as discussed in the following para.

In the present analysis, it has been observed that two concentric loops of secondary flows are formed within the back cavity (see Fig. 9 (a)). The outer loop of secondary flow, as mentioned earlier, moves in an anticlockwise direction. Interestingly, an inner secondary flow loop is also observed within the outer loop, but it moves in a clockwise direction. This inner loop is formed inside the outer loop and contributes to the overall flow pattern within the back cavity. The presence of these concentric loops of secondary flows indicates the complexity of the flow field and the intricate fluid dynamics occurring in the back cavity during reverse mode operation. Understanding the behavior and interaction of these secondary flow loops is crucial for analyzing the flow physics and associated losses in the back cavity. It provides valuable insights into the flow control mechanisms and guides the optimization of PAT design to minimize energy losses and enhance performance.

2) Formation of a mixing zone: The fluid that moves radially outward from the back cavity due to centrifugal force is pushed by the high-pressure inlet flow from the volute, resulting in the formation of a mixing region at the impeller inlet on the back shroud as shown in Fig. 9,

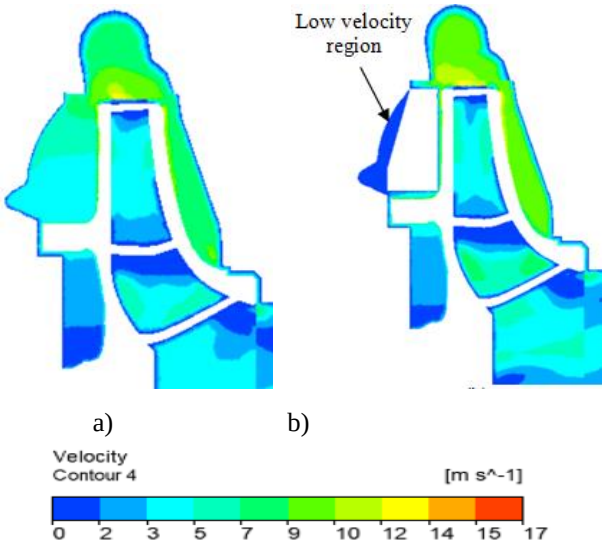

Fig. 10 Velocity contours at the meridional plane at BEP (a) without BCF and (b) with BCF

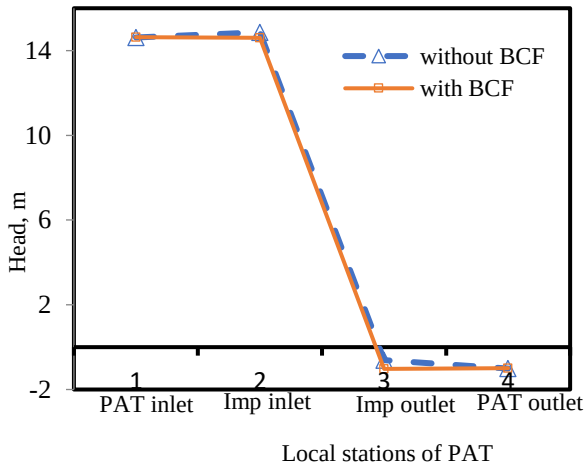

Fig. 11 Head at different local stations of PAT at BEP

first proposed by Doshi et al. (2018) in reverse mode operation of a pump based on investigations of experimental results along with the analytical model. As shown in Fig. 5, without BCF stage, there is enough space radially and axially (Gap A and B) to interact the back cavity and main flow, and through this space the fluid in the back cavity due to centrifugal force move radially outward direction. At the same instant, the fluid with high pressure head enters into the impeller. The interaction of these two flows in opposite direction is forming the vortices in the mixing region, which is having an effect on the entering flow into blade passages as shown in Fig. 9. Without BCF stage, the size of the vortices are significant and has higher pressure region, pushing the fluid entering towards the main flow zone, which may further results in flow separation in the blade passages, increasing the hydraulic losses mainly friction and wake formation.

In totality, the fluid in the back cavity is having influence not only in increasing the disk friction losses in the cavity but also influences the flow zone in large, affecting the performance of the PAT adversly.

After modifying the PAT with BCF, the secondary flow-based disk friction losses are significantly reduced. These reductions in losses are observed in Fig. 9 (b), which can be attributed to the reduction in the size of the cavity. As a result, the mass of fluid in the cavity is decreased, leading to the elimination of secondary flow within it. The reduction in losses resulted in an increase in shaft torque from 11 m to 11.6 m, indicating a 5.5 % improvement. However, it is also noted that the required head of the PAT is increased by 1.15 %. To understand this phenomenon, it is necessary to examine the distinct internal flow physics at the back cavity and the entry of the impeller.

Figure 10 illustrates that the reduction in the size of the back cavity causes a decrease in the mass of fluid present in it. Consequently, the fluid moves with lower velocity compared to the configuration without BCF, radially moving outwards from the back cavity. This reduction in velocity reduces the interference of the back cavity flow with the main flow in the mixing zone. As reported by Doshi et al. (2018), the increase in shaft torque (0.6 m of water head) is greater than the decrease in disk friction losses (0.27 m). This suggests that there is other favorable flow hydraulics contributing significantly to the increase in shaft torque.

The modification of BCF drastically reduces the flow from the back cavity, resulting in less resistance to the incoming high head flow. This reduction in resistance reduces the size of vortices and shifts their location towards the volute casing, minimizing their adverse effects on the main flow. The modified path for the main flow experiences reduced disturbances, resulting in a decrease in the required head at the impeller inlet. This result is supported by the Fig. 11, determining pressure head at various locations of the PAT (PAT inlet, impeller inlet, impeller outlet and PAT outlet), a method commonly used in the pump industry to understand the losses and their consequences on the head (in this, local stations are created in the geometry where pressure to be evaluated). As depicted in Fig. 11, at the impeller inlet, the required head with BCF stage is less than without BCF stage by the visible margin (-0.26 m) indicating the reduction in losses at the impeller inlet. This, in turn, increases the work transfer by the fluid as it passes through the impeller, subsequently enhancing the runner's torque. Therefore, along with the reduction of disk friction losses, the increase in runner torque contributes to the enhancement of shaft torque.

Though the head at impeller inlet is decreased after BCF, the net required head of PAT is increased compared to without BCF. The reason of increase of total required head after BCF is discussed in this paragraph. The head increases due to increase of runner torque and/or increase in the flow zone losses (Doshi et al., 2018). To understand the increase in required head, the change in the flow physics at impeller flow zone plays a key role for without and with BCF stages of PAT. In both stages, the large backward curved impeller blade causes the flow to strike the impeller pressure side (PS) towards the impeller inlet and then gets reversed,

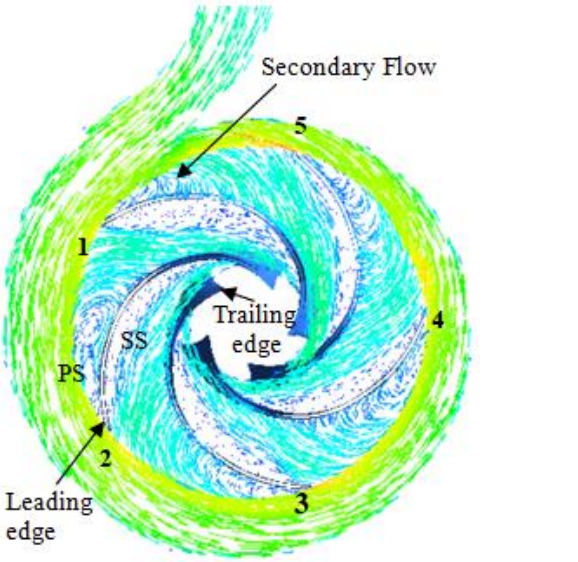

a)

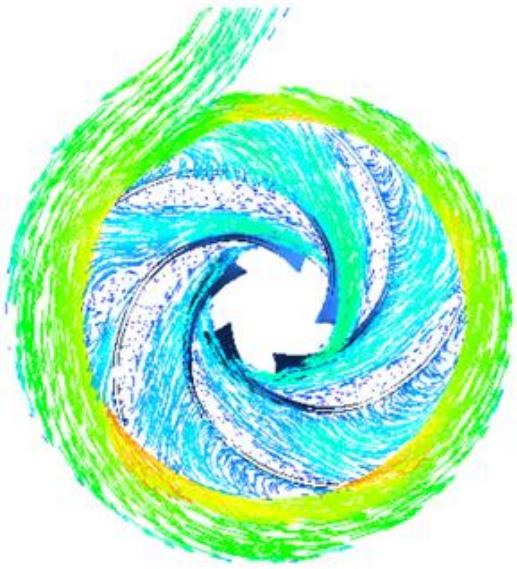

b)

PS: Pressure side; SS: Suction side

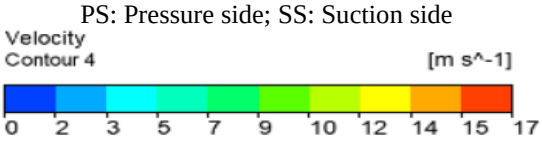

Fig. 12 Velocity vectors at impeller mid plane at BEP (a) without BCF and (b) with BCF

resulting in the formation of a secondary flow as shown in Fig. 12 (a). On the blade suction side (SS), the flow angle is not aligned with the impeller blade inlet tip since the impeller is not designed to work as a turbine. As a result, the flow separates from the impeller tip, creating a wake as shown in Fig. 13 (a). The location of the secondary flow and wake remains the same throughout, but their characteristics vary at different blade positions.

At blade 1 (marked in Fig. 12), the secondary flow region is low and occupies a shorter blade length. At blade 2, the region of secondary flow with vortex is relatively larger and covers more blade length from the blade leading edge. At blade 3, the secondary flow is similar to blade 1. While, at blade 4-5, the vortex in the

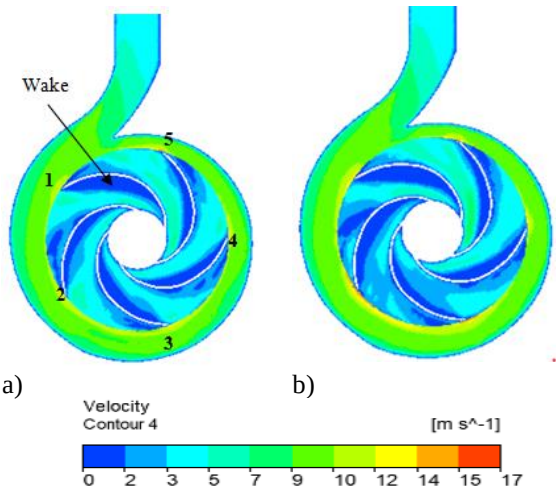

Fig. 13 Velocity contours at impeller mid plane at BEP (a) without BCF and (b) with BCF

secondary flow is less pronounced, but, covers the maximum blade length (from leading edge to trailing edge) with a relatively smaller width. Overall, the secondary flow and wake characteristics depend on the specific blade positions and the interaction between the impeller and the flow. Understanding these variations is important for optimizing the design and performance of the system.

Comparing the without and with BCF modification stages, the flow physics at the impeller flow zone is adversely affected. The secondary flow and wake is increased as shown in Fig. 12 (b) and 13 (b) compared to Fig. 12 (a) and 13 (a) respectively.

The flow passage between blade positions 1-2 and 2-3 is predominantly occupied by the secondary flow and wake. These adverse flow conditions lead to an increased required head. Therefore, the increase in the flow zone losses also contributed to the increment in the head. Though increase in the required head is still lower than the net increase in shaft torque (difference between the increase in torque and reduction in disk friction losses, 0.27 m) for both without and with BCF, resulting in dominant effect of performance improvement of PAT. Therefore, increase in shaft torque dominates the increase in head leads to an increase in efficiency from 66.7 % to 70.2 % (a relative increase of 3.5 %) for 19.9 rpm PAT studied in this work.

The analysis of Fig. 14-16 indicates the effects of the BCF modification on the pressure distribution and performance of the PAT. From the Fig. 14, the pressure contour plot illustrates that after implementing the BCF modification, the pressure at the back cavity decreases and becomes more uniformly distributed. This indicates a more balanced pressure distribution within the cavity. As shown in Fig. 15, the net pressure from the PAT inlet to outlet continuously decreases as expected. However, Fig. 15 (b) specifically shows a greater reduction in pressure at the impeller eye for the configuration with the BCF stage. This indicates that the modification has a more pronounced impact on reducing pressure at the impeller eye region.

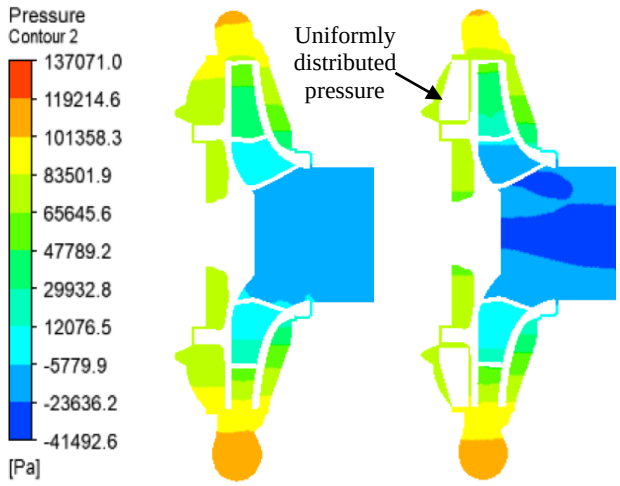

Fig. 14. Pressure contours at the meridional plane after BCF modification at BEP (a) without BCF and (b) with BCF

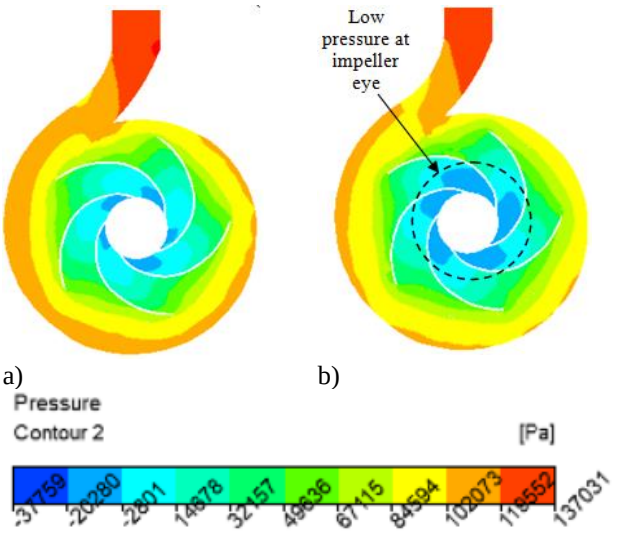

Fig. 15. Pressure contours at the mid plane of impeller at BEP (a) without BCF and (b) with BCF

As illustrated in Fig. 16, it is evident that the pressure is uniformly distributed over larger surface of the blade pressure side with the incorporation of the BCF stage, in contrast to the configuration without it. This suggests a redistribution of pressure across the blade surface due to the modification. Fig. 16 reveals a low-pressure region at the blade trailing edge after the implementation of the BCF. The negative pressure observed at the PAT outlet, measured relative to the reference atmospheric pressure. The uniform pressure distribution after BCF stage is noticed during the experimentation by more smoother operation with lower noise though it need to be quantified appropraite with consideration of force and vibration analysis.

Overall, the reduction of disk friction losses, the interaction of back cavity flow with the main flow, and alteration of the mixing region due to the implementation of BCF led to a net improvement in the performance of the PAT.

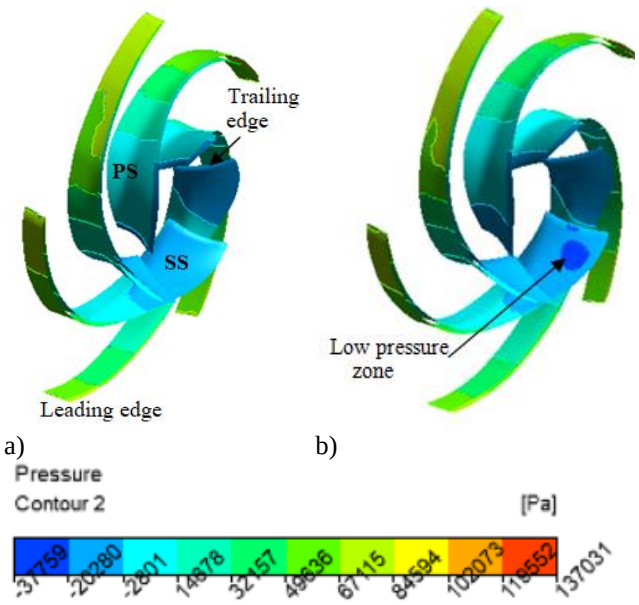

Fig. 16 Pressure on blade surface at BEP (a) without BCF and (b) with BCF

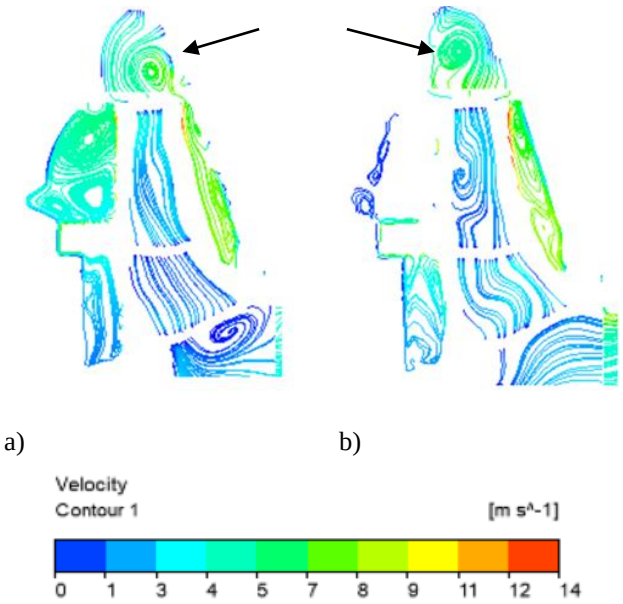

Fig. 17 Streamlines at meridional plane at part load condition (a) without BCF and (b) with BCF

4.3.2 Internal Hydraulics at Part Load and Overload Condition

The internal hydraulics at the part load and overload conditions differ significantly from the BEP. At the part load condition (lower than 16.9 lps, taken at Q=8.7 lps), the flow rate and pressure head are significantly lower compared to the BEP. The secondary flow is developed in the back cavity. But, instead of two concentric loops as observed for BEP, entire back cavity is occupied by three small loops of secondary flow formed seperately as shown in Fig. 17 (a). After the BCF modification, these secondary flow-based disk friction losses are reduced (refer Fig. 17 (b)) (as discussed in section 4.3.1), resulting in a significant increase in shaft torque from 3.2 m to 4.1 m (+28 %). Further, as depicted in Fig. 17,

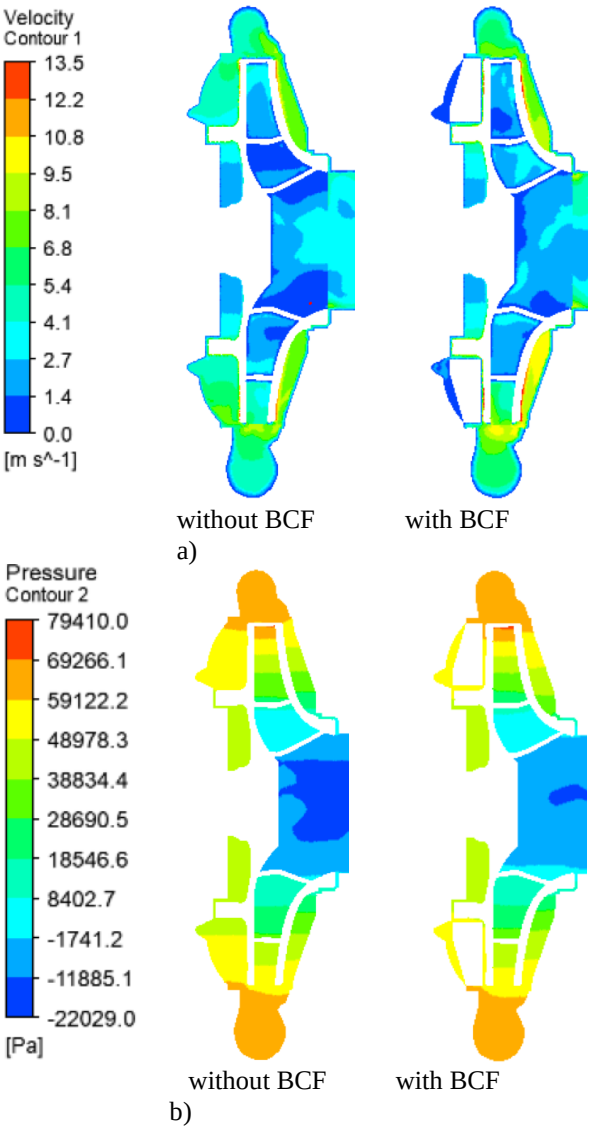

Fig. 18 Velocity and pressure contours at meridional plane at part load condition (a) velocity contours and (b) pressure contours

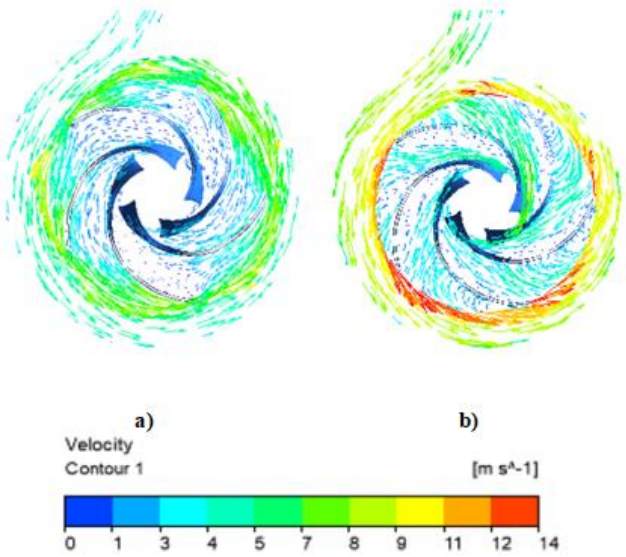

Fig. 19 Velocity contours at impeller mid plane at part load condition (a) without BCF and (b) with BCF

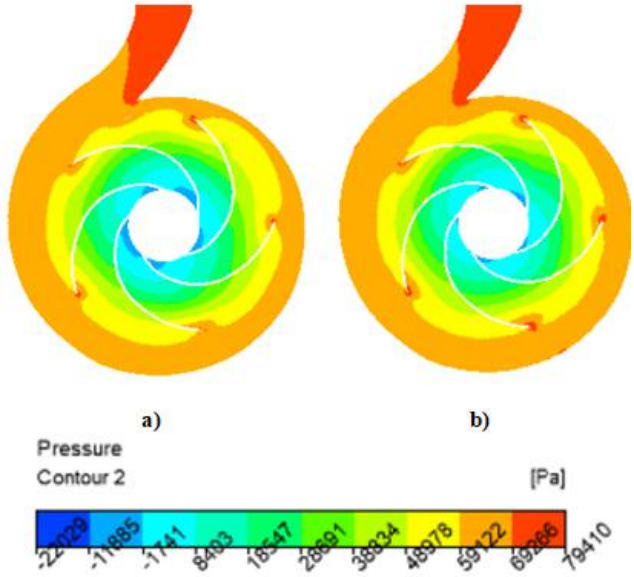

Fig. 20 Pressure contours at impeller mid plane at part load condition (a) without BCF and (b) with BCF

more vortices are observed at the volute (Kye et al. 2018). Fig. 18 illustrates that the change in velocity and pressure at meridional plane of PAT is nearly same as observed for BEP for without and with BCF.

In contrast to the BEP, after the BCF modification, the head of the PAT is decreased by small margin of 2.2 %. The internal hydraulics of the impeller flow zone is favorably changed after the modification. As shown in Fig. 19, the large wake is observed for without BCF stage, which is reduced after the BCF modification. Similar to the BEP, a low-pressure zone is observed at the impeller eye for both stages. The pressure concentration at the blade inlet tip is observed for both the stages, as shown in Fig. 20. Overall, the increase in shaft torque and decrease in head is resulted in an 11.2 % (absolute) increase in PAT efficiency.

Overload condition: At the overload condition (Q = 19.1 lps, greater than 16.9 lps), there is a noticeable presence of a large secondary flow in the back cavity, as shown in Fig. 21 (a). Further, large mixing zone is clearly visible at the impeller inlet shroud and extended at the entry of main flow into the impeller. Due to the implementation of the BCF modification reduction of the secondary flow-based disk friction losses are observed, as depicted in Fig. 21 (b). Consequently, the shaft torque increases from 13.1 m to 13.8 m, representing a 5.34 % improvement. The flow physics at the volute is complex due to formation of more vortices compared to the part load and BEP as shown in Fig. 21 and Fig. 22.

As depicted in Fig. 23, the secondary flow and wake are increased after the modification, leading to a 1 % increase in head. Efficiency of PAT at this stage is increased by 2.6 %. When comparing the BCF modification with the BEP and part load conditions, it is

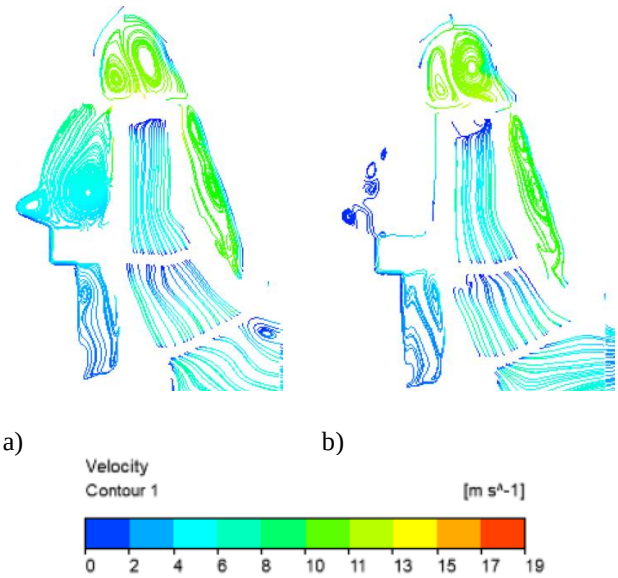

Fig. 21 Streamlines at meridional plane at overload condition (a) without BCF and (b) with BCF

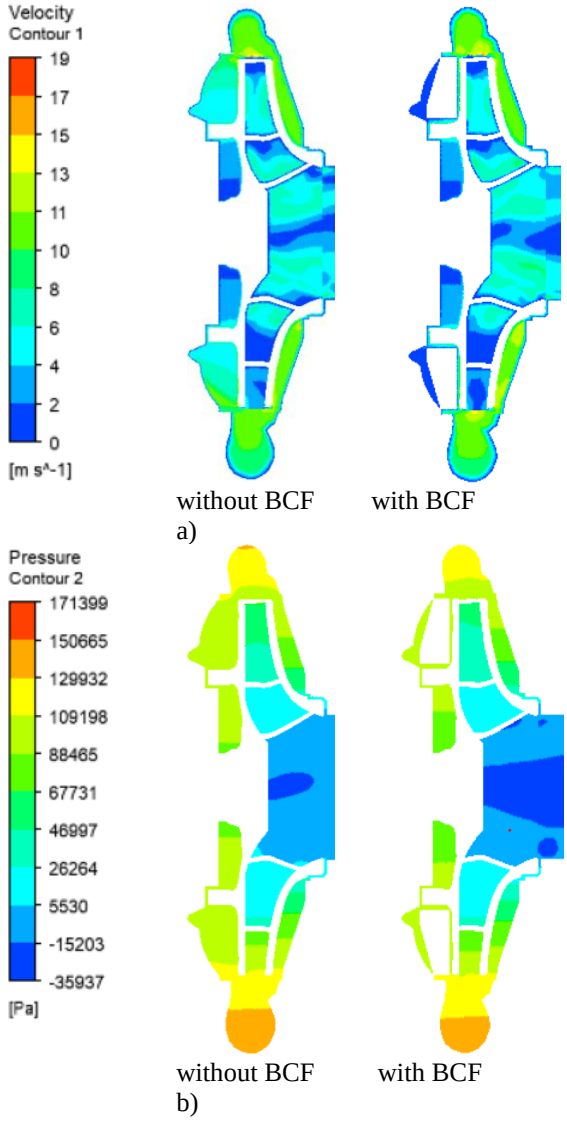

Fig. 22 Velocity and pressure contours at meridional plane at overload condition (a) velocity contours and (b) pressure contours

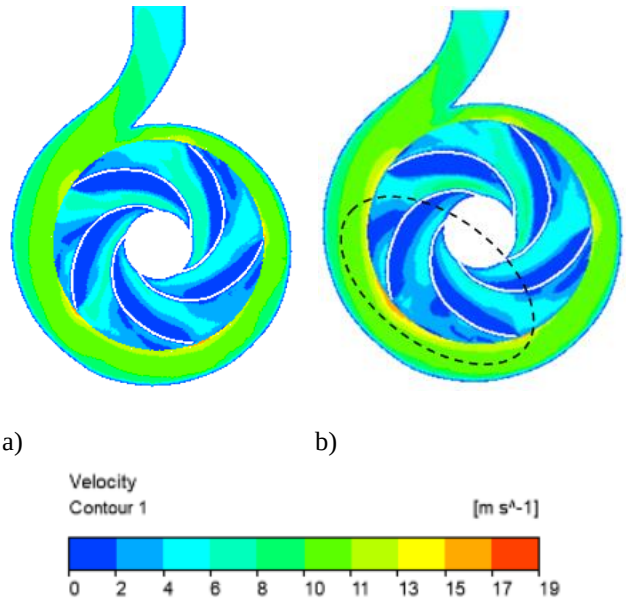

Fig. 23. Velocity contours at impeller mid plane at overload condition (a) without BCF and (b) with BCF

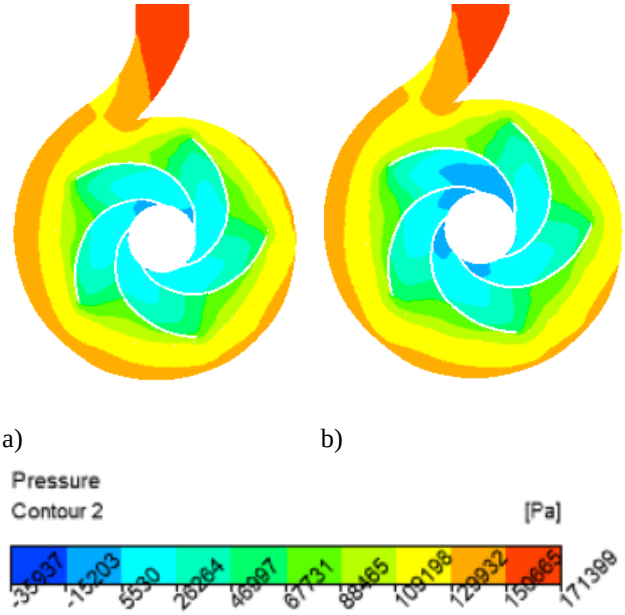

Fig. 24. Pressure contours at impeller mid plane at overload condition (a) without BCF and (b) with BCF

observed that the pressure at the back cavity is higher. However, the pressure is not significantly changed at the meridional plane after the BCF modification (refer to Fig. 22 (b)). Nevertheless, a slight reduction in pressure at the impeller eye is observed at the impeller mid-plane, as shown in Fig. 24.

4.4 Influence of Variation of Axial Clearance of Back Cavity on the Internal Hydraulics and Performance of 19.9 rpm PAT

To analyze the effect of size and shape of the back cavity on the PAT performance, the axial clearance of the back cavity is adjusted by incorporating different sizes of filling material in numerical simulations. Initially, the

Table 3 Performance parameters at different e

Axial clearance (mm)	e	Shaft torque (m)	Head (m)	Disk friction losses (m)	Efficiency (%)
2 (maximum size BCF)	0.015	11.64	16.59	0.95	70.2
4	0.03	11.48	16.52	1.02	69.48
6	0.058	11.35	16.49	1.09	68.84
8	0.061	11.16	16.44	1.09	67.89
10	0.076	11.10	16.41	1.12	67.63
24.6 (without BCF)	0.19	11	16.4	1.22	66.7

back cavity is filled with material of appropriate shape with an axial clearance of 2 mm (with BCF stage) between the ring and impeller shroud, as shown in Fig. 5 (b), for which investigation results are already presented in Sections 4.2 and 4.3. On the similar line, simulations are performed by increasing the axial clearance in the step of 2 mm, ranging from 2 mm to 10 mm there by reducing thickness of the back cavity filling material. The disk friction losses at different axial clearances are evaluated using the theoretical model proposed by Daily and Nece (1960) and used by Doshi et al. (2018). The results are summarized in Table 3 for various values of axial clearance in the non-dimensional form (e = axial clearance/impeller radius) with the performance parameters.

According to the Table 3, as the axial clearance (e) increases from 0.015 to 0.076, the shaft torque decreases from 11.64 m to 11.1 m, representing maximum 4.6 % reduction. Similarly, the head is also reduced from 16.59 m to 16.41 m, indicating a 1.1 % decrease. In accordance with same change in axial clearance (0.015 to 0.076), the disk friction losses increased by 0.17 m (17.9 %). The net decrease in shaft torque is greater than the relative increase in disk friction losses for all cases of change in axial clearance. Reduction in the runner torque is highlighting the role of the mixing zone as explained for maximum BCF case (base case). Although there is a reduction in both shaft torque and required head, the reduction in shaft torque outweighs the reduction in required head, resulting in a deterioration of the PAT efficiency by 2.6 % (absolute) with increase in the axial clearance from 0.015 to 0.076. The changes in flow physics at different axial clearance provide insights into the variations in PAT performance, which will be further discussed in the subsequent paragraphs.

Compared to e=0.015, at e=0.03, the clearance between the impeller shroud and the stationary ring is large, increased volume of the fluid present in cavity space, which further increases centrifugal force and thus velocity of it, and further increases the entry of volute fluid into the back cavity. Consequently, the secondary flow-based disk friction losses are increased (+7.36 %), results into decrease in shaft torque. On the other hand, head is also reduced by small margin. A small mixing region at the impeller inlet tip towards the volute side is observed, as shown in Fig. 25 (a).

At e=0.058, the increased axial clearance led to a higher interaction of volute fluid with the fluid in the back cavity. This resulted in the initiation of a small

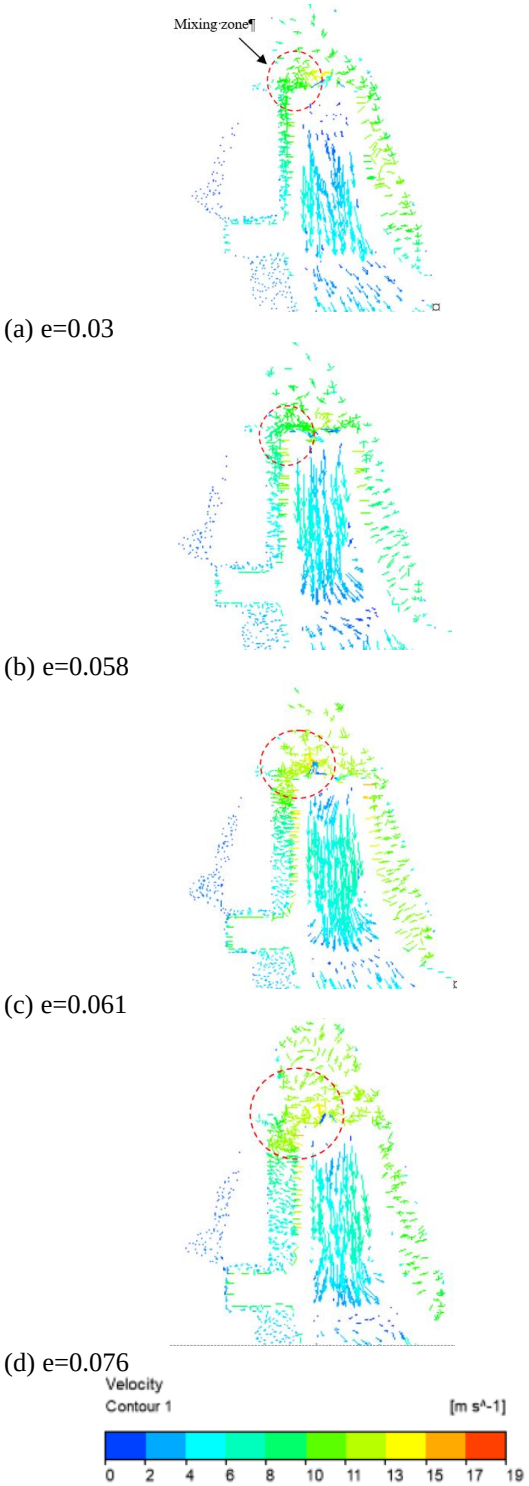

Fig. 25 Velocity vectors at different e at the meridional plane

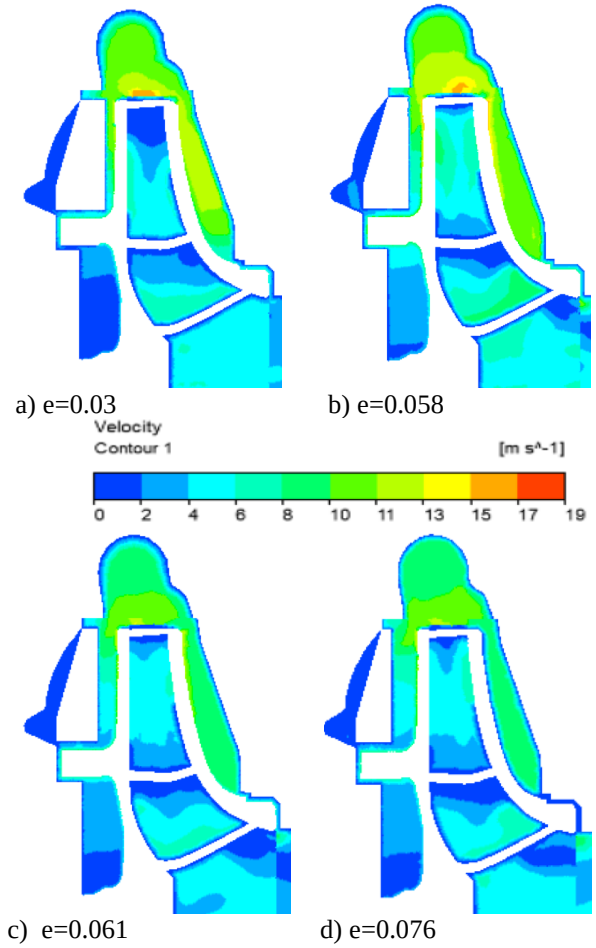

Fig. 26 Meridional plane velocity contours at different e at BEP

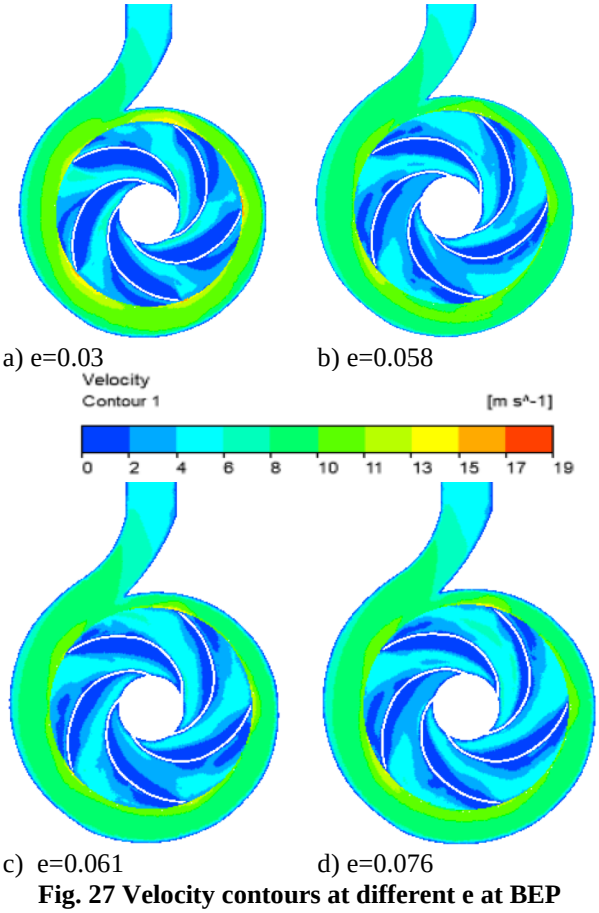

Fig. 27 Velocity contours at different e at BEP

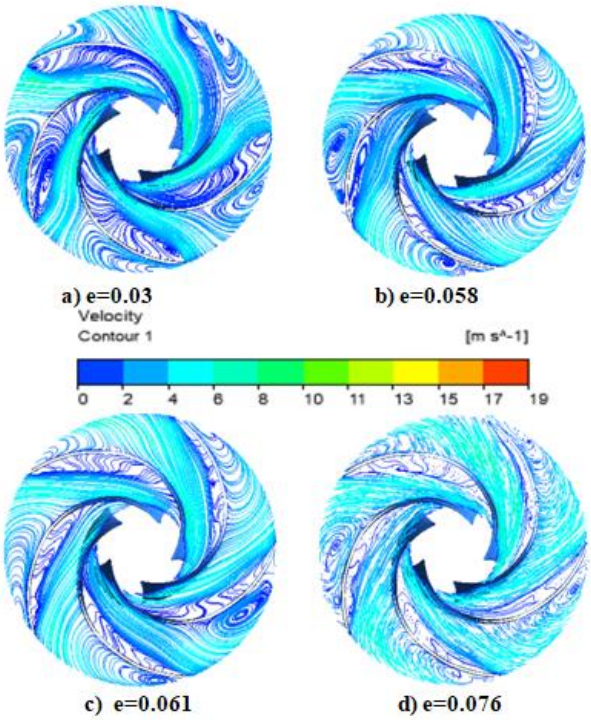

Fig. 28 Streamlines at impeller flow zone for different e at BEP

secondary flow loop at the back cavity, resulted into an increase in disk friction losses by 14.7 % compared to the baseline case at e=0.015. Additionally, the mixing region was expanded and shifted towards the impeller flow zone, as shown in Fig. 25 (b) and 26 (b), indicating higher velocities at the impeller inlet.

As e is further increased from 0.058 to 0.076, the secondary flow at the back cavity continued to intensify, leading to even higher disk friction losses and a consistent reduction in shaft torque. Moreover, the size of the mixing region increased with higher e, reaching its maximum extent at e=0.076. At e=0.061 and 0.076, the mixing region extended all the way to the entrance of the back cavity, as depicted in Fig. 25 (c-d) and Fig. 26 (c-d). But, the head continuously decreases with increasing e, primarily due to the decrease in wake and secondary flow at impeller flow zone, as presented in Fig. 27 and Fig. 28. Overall, the greater reduction in shaft torque compared to the decrease in head leads to a decrease in PAT efficiency.

In summary, varying the axial clearance in the back cavity has a significant impact on the PAT performance. Increasing the axial clearance leads to the formation of a mixing zone, resulting in increased disk friction losses, reduced shaft torque, and a decrease in PAT efficiency. The study provides valuable insights into the flow physics behind these changes and highlights the importance of optimizing the axial clearance to improve the performance of PAT. However, further discussions and analysis are required to fully understand the complex flow interactions and its impact on the velocity field in the radial and tangential direction of impeller and their implications for pump design and efficiency.

5. CONCLUSIONS

The influence of back cavity filling and its change in size by varying the axial clearance on the performance of a PAT along with flow physics was investigated using numerical simulations based on computational fluid dynamics (CFD). The numerical results for both with and without back cavity filling showed good agreement with the respective experimental data. The conclusions of this study are as follows:

1. Back cavity filling (BCF) not only reduced the disk friction losses caused by secondary flows at the back cavity but also having influence on the main flow zone in volute. Because of the free interaction of fluid in back cavity with the main flow at volute, after BCF modification the mixing region at the impeller inlet was reduced and shifted towards the outer side of volute and reduces the hydraulic losses due to friction and wake at the main flow zone. This led to a 3.5 % increase in PAT efficiency.
2. The analysis of variation in an axial clearance revealed that reduction of the thickness of the back cavity filling material (increasing the clearance from 0.015 to 0.076), resulted in 2.6 % decrease in PAT efficiency. The decline in performance is linked to an increase in disk friction losses caused by secondary flow within the back cavity. The location and size of the mixing zone depended on the axial clearance between the impeller back shroud and volute. As discussd, with an increased axial clearance, the size of the mixing region increased at impeller inlet, restricting the flow from the volute to the impeller flow zone. However, the increase in axial clearance slightly reduced the secondary flow and wake-based hydraulic losses at the impeller flow zone.
3. Overall, it is noticed that the design of axial clearance during reverse mode operation of a pump is an important geometric parameter as it affects the disk friction losses at the back cavity and hydraulic losses at the impeller inlet and impeller flow zone. The efficiency of the PAT can be increased by maintaining a low axial clearance. Visually, it is noticed due to this modification during experimentation more smoother operation of the PAT, but it is important to study thoroughly about the force analysis and it's effect on bearing and pump life.

Further research can be conducted to quantify the changes in hydraulic losses in both the flow zone and non-flow zone after modifying the axial clearance.

CONFLICT OF INTEREST

The authors declare that they have no conflicts of interest related to this research. This work was conducted with the highest level of integrity and objectivity. No financial support, direct or indirect, was received that could have influenced the design, execution, or interpretation of the study.

CONTRIBUTIONS OF THE AUTHOR

Rahul Gaji: Numerical Simulation, Validation, Investigation, Visualization. **Ashish Doshi:** Conceptualization, Resources, Experimentation. Theoretical model development. **Mukund Bade:** Conceptualization, Data curation, Writing – original draft, Data synthesis.

REFERENCES

Ayad, A. F., Abdalla, H. M., & El-azm, A. A. (2015). *Study of the effect of impeller side clearance on the centrifugal pump performance using CFD.* In Proceedings of the ASME 2015 International Mechanical Engineering Congress and Exposition, https://doi.org/10.1115/IMECE2015-50756.

Binama, M., Sua, W., Xiao-Bin L., Lia, F., Wei, X., & Shi,A. (2017). Investigation on pump as turbine (PAT) technical aspects for micro hydropower schemes : A state-of-the-art review. *Renewable and Sustainable Energy Reviews*, *79*, 148–179. https://doi.org/10.1016/j.rser.2017.04.071.

Cheng, Z., Ma, Q., Liu, H., Dong, L., & Pan, Q. (2023). Influence of dynamic and static interference on the internal flow and vibration and noise characteristics of marine centrifugal pump. *Journal of Applied Fluid Mechanics*, *16*(10), 1989-2001. https://doi.org/10.47176/JAFM.16.10.1860.

Daily, J., & Nece. R.. (1960). Chamber dimension effects on induced flow and frictional resistance of enclosed rotating disks. *Journal of Basic Engineering*, *82*(1) 217-230. https://doi.org/10.1115/1.3662532.

Doshi, A., Channiwala, S., & Singh, P. (2017). Inlet impeller rounding in pumps as turbines: An experimental study to investigate the relative effects of blade and shroud rounding. *Experimental Thermal and Fluid Science*, *82*, 333–348. https://doi.org/10.1016/j.expthermflusci.2016.11.024.

Doshi, A. V. (2018). *Influence of inlet impeller rounding and the shape of non flow zones on the performance of centrifugal pump as turbine*. [Ph.D thesis, SVNIT], India.

Doshi, A. V., Channiwala, S., & Singh, P. (2018). Influence of non-flow zone (back cavity) geometry on the performance of pumps as turbines. *Journal of Fluids Engineering*, (10.1115/1.4040300). https://doi.org/10.1115/1.4028225.

Gaji, R., Doshi, A., Bade, M., & Singh P. (2023). Influence of impeller blade rounding and surface roughness on the internal hydraulics and performance of pump as turbine. *Archive of Mechanical Engineering*, *70* (2) 219-245. https://doi.org/10.24425/ame.2023.145581.

Gülich, J. F. (2013). *Centrifugal Pumps*. Springer. 3rd edition. https://doi.org/10.1017/CBO9781107415324.004.

Javadi, A., & Nilsson, H. (2017). Detailed numerical

investigation of a Kaplan turbine with rotor-stator interaction using turbulence-resolving simulations. *International Journal of Heat and Fluid Flow*, 63, 1–13. https://doi.org/10.1016/j.ijheatfluidflow.2016.11.010.

Kye, B., Park, K., Choi, H., Lee, M., & Kim, J. (2018). Flow characteristics in a volute-type centrifugal pump using large eddy simulation. *International Journal of Heat and Fluid Flow*, *72*(April), 52–60. https://doi.org/10.1016/j.ijheatfluidflow.2018.04.016.

Li, Q., Zhang, R., & Xu, H. (2023a). Effects of volute structure on energy performance and rotor operational stability of molten salt pumps. *Journal of Applied Fluid Mechanics*, *16*(8), 1615-1626. https://doi.org/10.47176/JAFM.16.08.1741

Li, W., Huang, Y., Ji, L., Ma, L., Agarwal, R., Awais, M. (2023b). Prediction model for energy conversion characteristics during transient processes in a mixed-flow pump. *Energy*, *271* (127082). https://doi.org/10.1016/j.energy.2023.127082.

Li, W., Liu, M., Ji, L., Li, S., Song, R., Wang, C., Cao, W., Agarwal, R. (2023c). Study on the trajectory of tip leakage vortex and energy characteristics of mixed-flow pump under cavitation conditions. *Ocean Engineering*, *267* (301). https://doi.org/10.1016/j.oceaneng.2022.113225.

Miao, S., Yang, J., Shi, G., & Wang, T. (2015). Blade profile optimization of pump as turbine. *Advances in Mechanical Engineering*, *7*(9), 1–9. https://doi.org/10.1177/1687814015605748.

Singh, P. (2005). *Optimization of internal hydraulics and of system design for pumps as turbines with field implementation and evaluation*. [Ph.D thesis, University of Karlsruhe], Germany. https://doi.org/10.1.1.459.9416.

Singh, P., & Nestmann, F. (2011). Internal hydraulic analysis of impeller rounding in centrifugal pumps as turbines. *Experimental Thermal and Fluid Science*, *35*(1), 121–134. https://doi.org/10.1016/j.expthermflusci.2010.08.013.

Suarda, M., Suarnadwipa, N., & Adnyana, W. B. (2006). *Experimental work on modification of impeller tips of a centrifugal pump as a turbine*. Sustainable Energy and Environment (SEE 2006), Bangkok, Thailand.

Tian, P., Huang, J., Shi, W., & Zhou, L. (2019). Optimization of a centrifugal pump used as a turbine impeller by means of an orthogonal test approach. *Fluid Dynamics & Materials Processing*, *15*(2), 139–151. https://doi.org/10.32604/fdmp.2019.05216.

Yan, J., Zuo, Z., Guo, W., Hou, H., Zhou, X., & Chen, H. (2019). Influences of wear-ring clearance leakage on performance of a small-scale pump-turbine. *J. Power and Energy*, *0*(11), 1–16. https://doi.org/10.1177/0957650919865052.

Yang, H., Zhu, L., Xue, H., Duan, J., & Deng, F. (2021). A numerical analysis of the effect of impeller rounding on centrifugal pump as turbine. *Processes*. *9*(9), 1673. https://doi.org/https://doi.org/10.3390/pr9091673.

Yang, S., Kong, F., Jiang, W., & Qu, X. (2012a). Effects of impeller trimming influencing pump as turbine. https://doi.org/10.1016/j.compfluid.2012.07.009.

Yang, S., Kong, F., Fu, J., & Ling, X. (2012b). Numerical research on effects of splitter blades to the influence of pump as turbine. *International Journal of Rotating Machinery*, 2012, Article ID 123093, 9 pages https://doi.org/10.1155/2012/123093.

Yang, S., Derakhshan, S., & Kong, F. Y. (2012c). Theoretical, numerical and experimental prediction of pump as turbine performance. *Renewable Energy*, *48*, 507–513. https://doi.org/10.1016/j.renene.2012.06.002.

Yang, S., Liu, H., Kong, F., Xia, B., & Tan, L. (2014). Effects of the radial gap between impeller tips and volute tongue influencing the performance and pressure pulsations of pump as turbine. *Journal of Fluids Engineering*, *136*, 1–8. https://doi.org/10.1115/1.4026544.

Zariatin, D. L., Rahmalina, D., Prasetyo, E., Suwandi, A., & Sumardi, M. S. (2019). The effect of surface roughness of the impeller to the performance of pump as turbine pico power plant. *Journal of Mechanical Engineering and Science*, *13*(1), 4693–4703. https://doi.org/10.15282/jmes.13.1.2019.24.0394.

Zemanová, L., & Rudolf, P. (2020). Flow inside the sidewall gaps of hydraulic machines: A review. *Energies*, 13(24). https://doi.org/10.3390/en13246617.

APPENDICES

Test Rig Instrumentation, Uncertainty and Repeatability

The measuring instruments used to determine external parameters such as pressure, flow rate, torque, and speed are detailed in Table A1. The absolute and relative uncertainties of various PAT performance parameters were evaluated at the BEP and 1000 rpm. A summary of the uncertainty is presented in Table A2. The precision of efficiency measurement is characterized by an absolute uncertainty of ± 0.37 (without BCF) and ± 0.39 (with BCF), while the relative uncertainty is ± 0.57 for both stages. The repeatability of the instruments was assessed by conducting two sets of readings, and the results were plotted using dimensionless parameters. Fig. A1 illustrates the close overlap of efficiency and head number for both sets, demonstrating the excellent repeatability of the measuring instruments.

Table A1 Measuring instruments and accuracy (Doshi, 2018)

Instruments	Parameters	Range	Accuracy
Pressure transmitter	Pressure at inlet	0 to 3.5 bar	±0.065% of the span
	Pressure at outlet	0 to -1 bar	±0.065 % of the span
Flow transmitter	Flow rate	0 to 50 lps	±0.5 % of full scale reading
Torque sensor	Torque	0 to 50 Nm	±0.05 % of full scale reading
Speed sensor	Speed	0 to 3000 rpm	±1 rpm

Table A2 Uncertainty in the measurement

Parameters	Notations	Without BCF	With BCF
Speed	ΔN (rpm)	±1	-
	ΔN/N (%)	±0.1	-
Discharge	Q (lps)	16.83	16.83
	ΔQ (lps)	±0.09	-
	ΔQ/Q (%)	±0.5	-
Head	H (m)	16.72	17.02
	ΔH (m)	±0.04	±0.03
	ΔH/H (m)	±0.2	±0.21
Torque	T (N-m)	17.12	18.37
	ΔT (N-m)	±0.025	±0.025
	ΔT/T (N-m)	±0.15	±0.14
Shaft torque	Shaft head (m)	10.79	11.58
	Δ Shaft head (m)	±0.06	±0.06
	Δ Shaft head / Shaft head (%)	±0.53	±0.53
Efficiency	η	64.55	68.15
	Δη	±0.37	±0.39
	Δη/ η	±0.57	±0.57

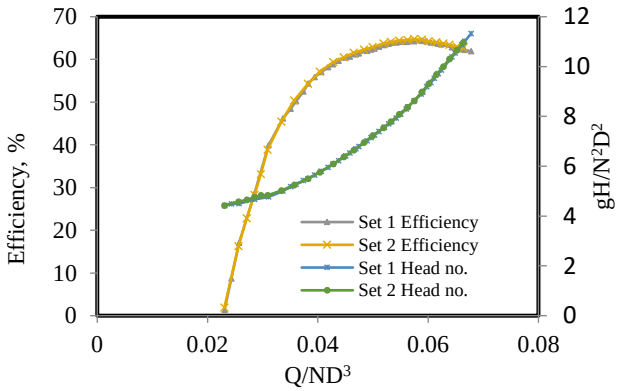

Fig. A1 Dimensionless PAT characteristic plot Relationship Between the Performance Parameters and Losses

The theoretical model is used to correlate the change in the internal flow physics of PAT flow control volumes (Doshi, 2018). The steady-state Euler's equations of the energy transfer in turbine mode under ideal conditions are presented by equations (B1) and (B2).

$$H_E = \frac{C_{u1}u_1 - C_{u2}u_2}{g} \tag{B1}$$

$$H_E = \left(\frac{\Delta(C_u u)}{g}\right)_{runner} \tag{B2}$$

Net head represented by equation (B3) is the energy measured across the inlet and outlet section of PAT, which includes the losses that occur in the flow zone.

$$H = \left(\frac{\Delta(C_u u)}{g}\right)_{impeller} + h_{L,fz} \tag{B3}$$

Shaft torque is measured at the PAT's end and obtained by subtracting the disk friction losses from the runner torque represented by equation (B4). The mechanical losses at the seals and bearing are not considered.

$$\frac{T\omega}{\rho Q g} = \left(\frac{\Delta(C_u u)}{g}\right)_{shaft} = \left(\frac{\Delta(C_u u)}{g}\right)_{runner} - h_{L,nfz} \tag{B4}$$

The net head across the PAT control volume calculated by combining equations (B3) and (B4) is expressed as,

$$H = \left(\frac{\Delta(C_u u)}{g}\right)_{shaft} + h_{L,fz} + h_{L,nfz} \tag{B5}$$